Journal of Inorganic and Organometallic Polymers and Materials (2022) 32:536–546
https://doi.org/10.1007/s10904-021-02156-1

Gamma Irradiation-Induced Preparation of Polyacrylonitrile Acrylamide Nano-silica for Removal of Some Hazardous Metals

Mohamed Ragab Abass[1] · Eman Hassan EL-Masry[1] · Wafaa Mohamed El-Kenany[1]

Received: 12 August 2021 / Accepted: 9 November 2021 / Published online: 17 November 2021

Abstract

Gamma-irradiation initiated polymerization was utilized to prepare polyacrylonitrile acrylamide nano-silica (P(AN-AM)-NS). Various analytical tools like XRD, FT-IR, SEM, TEM, and DTA and TGA were used to estimate the morphology, functional groups, and structure of P(AN-AM)-NS nanocomposite. The ability of P(AN-AM)-NS nanocomposite to remove Cs(I), Pb(II), Cd(II), Sr(II), and Cu(II) ions from the multi-component system was evaluated by batch techniques considering the influence of (shaking time, pH, reaction temperatures), and capacity. At the optimum pH, distribution coefficients have selectivity order; $Pb^{2+} > Cs^{+} > Cu^{2+} > Cd^{2+} > Sr^{2+}$. The kinetic data obey pseudo-second-order models. The capacity was reduced by increasing the heating temperatures of solid powder. The thermodynamic parameters showed an endothermic and spontaneous. The investigation proved that P(AN-AM)-NS nanocomposite is a suitable organic–inorganic sorbent for the sorption of the studied ions from liquid solutions and could be considered as potential material for purification of effluent polluted with these ions.

Graphical Abstract

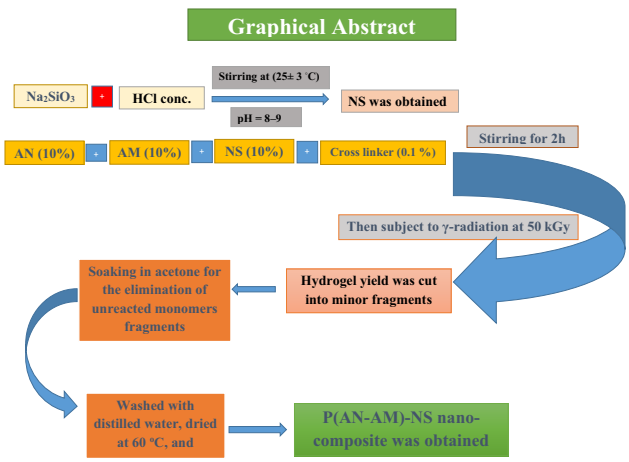

Keywords Gamma-irradiation · Polymerization · Nano-silica · Distribution coefficients · Kinetic · Thermodynamic

1 Introduction

Resin exchangers for environmental pollution remediation were widely used by different investigators [1–3]. Many organic and inorganic sorbents were reported with wide-ranging utility. Organic sorbents have impoverished thermal and radiation stability and are therefore unstable

✉ Eman Hassan EL-Masry
emanelmasry74@gmail.com

Extended author information available on the last page of the article

in strong radiation fields at high temperatures [4]. Inorganic exchangers are very stable towards high radiation and temperatures but are inadequate to treat huge volumes of radwaste and costly [5]. Thus, to solve restrictions related to both organic and inorganic sorbents, efforts were made for the combination of composite sorbents with enhanced properties [6]. Composite sorbents were produced by mixing polymers as supporting materials with inorganic species as an exchanger. The material is mechanically, thermally, and chemically more stable [7, 8]. The polymer in composite material improves the mechanical, optical characteristics and provides more exchangeable spots [9]. The composite sorbents had a strong interest due to their variation of usages in unlike fields such as water purification, chemical separation, electrochemical sensor, solar cell, optical properties, and catalyst [9, 10]. Many pollutants disrupt or change the chemical structure of water in the world and affect the aquatic environment [11]. The current methods for the sorption of hazardous metals from liquid waste solutions include chemical precipitation, ion exchange, membrane, adsorption, and biosorption [11–13]. Recently it is one of the biggest challenges to remove contaminants from wastewater, as their importance increases with growing industrial activities [2]. Studies on % uptake of Pb(II), Cs(I), Cu(II), Sr(II), and Cd(II) ions from liquid media have been focused largely on adsorption and ion exchange methods [14–19]. The potential toxicity and adverse health effects are shown by toxic metals such as Cd, Cu, Pb, Cs, and Sr ions. The novelty of this work includes impregnation of nano-silica inside polyacrylonitrile acrylamide layers initiated by gamma radiation as a new nanocomposite with high sorption performance for Pb(II), Cs(I), Cu(II), Sr(II), and Cd(II) ions from liquid solutions. Many years of research and development work in polymer radiation chemistry has led to many advantages of the gamma radiation polymerization process over other conventional methods. Ionizing radiation is widely applicable in modifying the structure of polymers and a significant advantage of the use of radiation is that the processes can be considered "solvent-free" for conventional synthesis procedures thereby reducing or avoiding the presence of additives that could be potentially harmful. The dose rate can be varied easily which makes the control of reaction easier and better. Chemical initiation has often been associated with problems arising from the local overheating of the initiator. The radiation processing, however, is temperature independent, which is therefore considered as a zero activation energy process for initiation. The advantage of the gamma radiation polymerization process is represented in gradient crosslinking, improvement of surface hardness of some polymers. Irradiation of polymer blends can be used to crosslink or degrade the desired component polymer, to fixate the blend morphology, Enhanced crosslinking, and reduce chain scission for amorphous regions of polymeric composites. The possibility of polymerizing monomers which are difficult to polymerize by conventional methods in radiation-induced initiation, the polymer is pure because in this case initiation is carried out by a fragment of the monomer molecule of the same chemical nature. Even the defects of this process represented in the possibility of the occurrence of secondary processes under the influence of ionizing radiation: crosslinking or degradation of the polymers, can be eliminated by selecting optimum polymerization conditions. However, in some cases, this defect may be regarded as an advantage of radiation-induced polymerization when it is desirable to combine in a single process the preparation and crosslinking of chain polymers [20]. In the current work, the sorption of hazardous metal ions Pb(II), Cs(I), Cu(II), Sr(II), and Cd(II) from liquid waste was investigated onto polyacrylonitrile acrylamide nano-silica prepared by gamma radiation technique at 50 kGy.

2 Experimental

2.1 Chemicals and Reagents

The main chemicals used to prepare P(AN-AM)-NS were Na_2SiO_3 (Loba Chemie, India), acrylonitrile (AN), acrylamide (AM), N, N-methylene bisacrylamide, and dimethyl ketone (α-Chemika, India). Chemical such as CsCl, $CuCl_2{\cdot}2H_2O$, $SrCl_2$, $PbCl_2$, $CdCl_2$, $AgNO_3$, HNO_3, and HCl (Merck, Germany) and KOH (El-Nasr, Egypt). Chemicals utilized in this article have an analytical assessment. For all tests, preparing solutions, double-distilled water (DDW) was employed. Measurements of the initial pH of studied metal ion solutions were completed utilizing a lab pH-meter, (pH 601A, (USA).

2.2 Gamma Cell

A Co^{60} γ-cell of class MC-20 (Russia), was applied as a radiation foundation for the polymerization process at the Cyclotron, Egypt. The solution was irradiated in a plastic bottle. The irradiation dosage rate was ~ 473.35 Gy/h.

2.3 Preparation

2.3.1 Fabrication of Nano-silica (NS)

As reported [21], NS was fabricated by addition of concentrated HCl (dorpwith) to Na_2SiO_3 solution with constant stirring at (25 ± 1 °C) until pH approximately (8–9), gel of silica was obtained and aged for one day, then decantation of filtrate from precipitate, accompanying washing with warm DDW sometimes until free from Cl^- that tested using $AgNO_3$ (dilute solution). After the drying at 80 °C, the NS

powder collected, white NS were ground for 300 s in fast mills.

2.3.2 Preparation of P(AN-AM)-NS

At 25 ± 1 °C and constant stirring, add drop by drop of 10% acrylonitrile (AN), acrylamide (AM), and nano-silica (NS) solutions, and N, N-methylene-bisacrylamide (0.1%) was developed for the production of P(AN-AM)-NS with volumetric ratios (AN:AM:NS) equal unity. The solution was agitated for 120 min to overcome complete homogeneity then subject to γ-irradiation at 50 kGy of about 4.38 days. After the radiation process, the gel yield was cut into minor fragments, soaking in dimethyl ketone for about 4 h with constant stirring to eliminate unreacted components, rinsed with DDW more than one times until pH reach 7, dried at 60 °C. The solid material was transformed into the hydrogen form by treating it for 24 h with 0.1 M HNO_3. The gel product was purified numerous times with DDW to confiscate the excess HNO_3 and dried at 60 °C.

2.4 Instruments

The studied material was analyzed with an IR spectrophotometer (Alpha II Bruker, Germany). XRD measurement is conducted (Shimadzu, Japan). The prepared nanocomposite was analyzed for TGA and DTA in N_2 atmosphere by a Shimadzu DTG-60 H. Direct observation via SEM examined the micrographs of the sample produced (model JSM-5400, JEOL Instrument, Japan). TEM was done using (JEM2100, Jeol. s.b, Japan).

2.5 Stability to Different Solvents

The stability of P(AN-AM)-NS to chemical attack was conducted by shaking 100 mg of nanocomposite and 100 mL of DDW, HNO_3, HCl, and KOH in a range of concentrations [1–6 M]. The solution with irregular shaking for about 4 days. The precipitate establish was detected gravimetrically [15].

2.6 Adsorption Investigations

2.6.1 Influence of Shaking Time

An equilibrium was done by shaking 0.1 g of solid in H^+ form with 10 mL of the multi-component system (Pb(II), Cs(I), Cu(II), Sr(II), and Cd(II) ions) in a shaker thermostat (Kottermann, Germany) at 25 ± 1 °C with batch factor (V/m = 100 mL/g). After each time interval, a shaker is fixed and the filtrate is removed at once from the solid. Hence, AAS was utilized to detect the tested ions concentration. The % removal can be known by the next equation [22, 23]:

$$\%\ \text{Removal} = \left(\frac{C_i - C_f}{C_i}\right) \times 100 \tag{1}$$

In which: C_i (initial concentrations) and C_f (final concentrations) of metal ions in solution.

2.6.2 Ion-Exchange Behavior

To examine the sorption of the multi-component system (Cs(I), Pb(II), Cu(II), Sr(II), and Cd(II) ions) using batch techniques, a sequence of experiments was applied at 100 mg/L for investigated cations at constant V/m = 100 mL/g and changed pH and 25 ± 1 °C. Both distribution coefficient (K_d) and separation factor (α_b^a) as a function of pH were calculated with the following equations [14]:

$$K_d\,(\text{mL/g}) = \left(\frac{C_i - C_f}{C_f}\right)\frac{V}{m} \tag{2}$$

$$\alpha_b^a = \frac{K_d\,(b)}{K_d\,(a)} \tag{3}$$

where V and m are the solution volume (L), and P(AN-AM)-NS weight (g), a and b are two competing types in a system.

The kinetic analysis for the investigated cations onto the P(AN-AM)-NS in H^+ form was taken place by applying the solid with investigated cations (100 mg/L) with a V/m ratio of 100 mL/g at the wanted pH in a shaker thermostat at 25 ± 1 °C.

The influence of different reaction temperatures (25–65 °C) on the amount of sorbed ions (q). In each experiment, 10 mL of investigated metal ions at desired pH, and 0.1 g of solid in H^+ form at V/m = 100 mL/g was vigorously shacked for 4 h using a thermostatic water bath shaker. The solution's pH has been adjusted with NaOH and/or HCl for all investigations.

2.6.3 Capacity Measurements and Thermal Stability

Batch equilibration repeated for investigated cations (200 mg/L) with the solid sorbent in V/m = 100 mL/g was applied for the capacity estimation at different heating temperatures (50–400 °C) in a muffle kiln for 4 h. The multi-component systems (Cs(I), Pb(II), Cu(II), Sr(II), and Cd(II) ions) were agitated in a shaker thermostat at pH 4.3 for 4 h. The capacity was calculated from Eq. (4) [24, 25].

$$\text{Capacity} = \frac{(C_i - C_e)V}{m}\ mg/g \tag{4}$$

3 Results and Discussion

The object of this article is the effort to produce a great chemical stable organic–inorganic hybrid nanocomposite with a great affinity to Pb(II), Cs(I), Cu(II), Sr(II), and Cd(II) cations from liquid solutions. Polyacrylonitrile acrylamide nano-silica was fabricated by γ-irradiation within 50 kGy with comprehensive characterization.

3.1 Characterization

3.1.1 FT-IR

IR spectrum of P(AN-AM)-NS nanocomposite (Fig. 1). This figure shows that broadband was noticed at 3470–3300 cm^{-1} due to H_2O (stretching vibration) and OH adsorbed on P(AN-AM)-NS [26]. Two bands were noticed at 3190 and 2940 cm^{-1} due to N–H (stretching vibration) and CH_2, respectively, [27–29]. A strong absorption band at 2244 cm^{-1} due to the C≡N bond of AN (stretching vibration) [30]. 2 bands at 1661 and 1605 cm^{-1}, corresponding to amide I (stretching vibration) [31], and N–H of AM (bending vibration) or O–H bonded H_2O absorbed on P(AN-AM)-NS [27, 32]. The band appeared at 1571 cm^{-1} related to the C–N–H bond (bending vibration) [31]. 2 bands appeared at 1451 and 1413 cm^{-1} related to an asymmetric and symmetric CH_2 (bending vibration) [27, 33]. 2 bands at 1340 and 1220 cm^{-1} related to asymmetric and symmetric C–N (bending vibration) [31]. The bands appeared at 1040 and 905 cm^{-1} attributed to Si–O–Si and Si–O–H deformation vibration, respectively [34]. The bands at 636 and 460 cm^{-1}, attributed to Si–O [26].

3.1.2 XRD Analysis

XRD analysis of P(AN-AM)-NS (Fig. 2). It is clear that the prepared material has a crystalline structure and this result

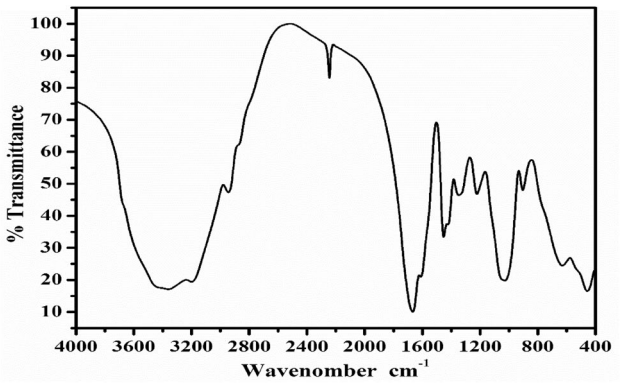

Fig. 1 IR spectrum for P(AN-AM)-NS nanocomposite

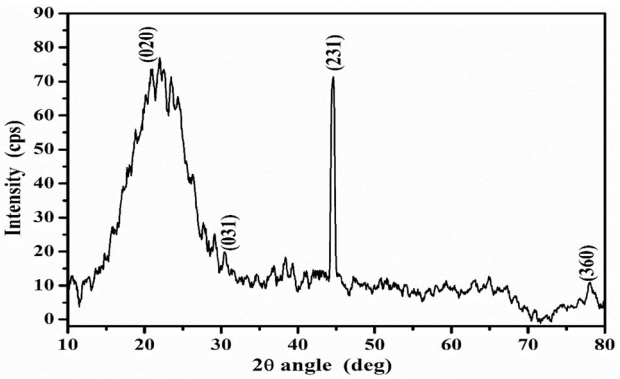

Fig. 2 XRD analysis for P(AN-AM)-NS nanocomposite

was parallel to the data acquired from XRD of {P(AM-AA)-MgSi} [9] and (KCFC–PAN) [35]. It can be established that the unlike indexed peaks at 30.6°, 45.1°, and 77.7° correspond to (031), (231), and (360) in P(AN-AM)-NS patterns (XRD JCPDS data file no. 43–1022) [9], a representative that it is supplemented with crystalline moieties. The motive for this is related to the presence of NS in P(AN-AM)-NS. Another peak looking at 20.9° corresponds to (020) is cross-banding to the occurrence of AM [9].

3.1.3 Thermal Analysis

DTAandTGA chart of P(AN-AM)-NS (Fig. 3), via a three-steps. From 47 to 225 °C due to the reduction of surface moisture of polymeric resin [9], the weight loss is 10.5%. From 225 to 505 °C due to the removal of H_2O of crystallization [3] and complete decay of the organic portion of the powder [36], the lost weight is 33.2%. From 505 to 700 °C due to heating in N_2 consequences in a cyclization reaction with nitryl bonds converted to C = N [36], the weight loss is 18.1%. DTA displays that peak at 92 °C (endothermic) was attributed to the removal of surface moisture of polymeric resin. Two exothermic peaks appear at (353 and 533 °C), respectively, corresponding to the widespread decomposition of the organic fragment or due to heating in N_2 consequences in a cyclization reaction with nitryl bonds converted to C = N. From TGA data (Fig. 3), the lost weight is continuous up to 600 °C. This supporting the fact that P(AN-AM)-NS has good thermal steadiness comparing with the different polymeric resins and the full lost weight with a heating temperature of 61.9%.

3.1.4 Morphology Structures (SEM)

Micrograph of P(AN-AM)-NS nanocomposite Fig. 4A showed an irregular, homogenous distribution of a large number of nanospheres spherical nanocomposite with the construction of a large number of cavities on the surface,

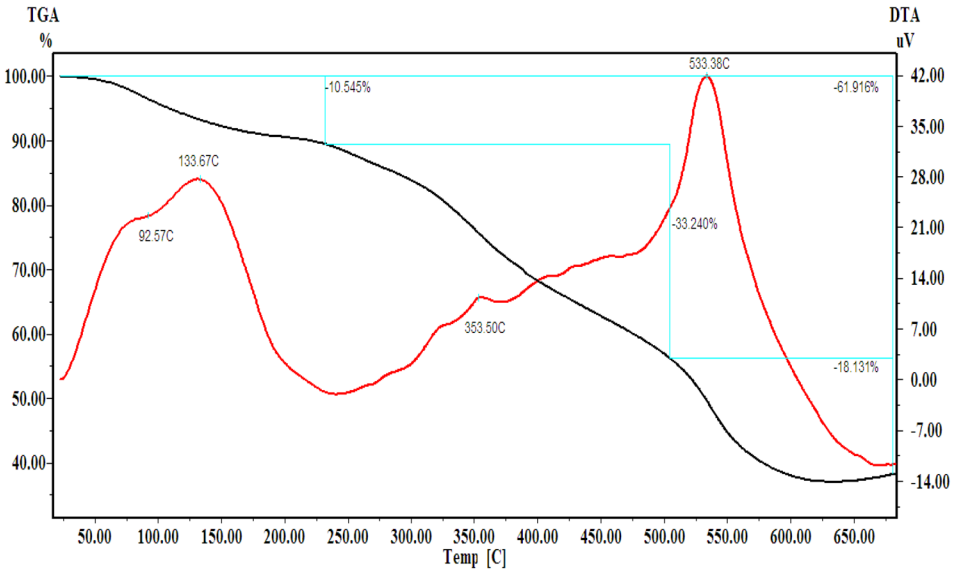

Fig. 3 TGA and DTA analysis for P(AN-AM)-NS nanocomposite

which makes it easier to bring more active adsorption spots [29, 30, 37–39].

3.1.5 TEM

Transmission electron micrographs of P(AN-AM)-NS nanocomposite presented in Fig. 4B, C, exposed the presence of spherical units with sizes ranged from 2.3 to 4 nm. TEM images also showed no aggregations formation [40]. An experimentally noticed diffraction pattern viewing the central, intense, direct beam such a pattern, with a sharply intensive spot indicating that the specimen is at least moderately crystalline [41].

3.2 Chemical Stability

The stability of P(AN-AM)-NS to chemical attack was studied in different solvents (H_2O, HNO_3, HCl, and KOH) and the results are tabulated in Table 1 and indicated that the prepared sample is stable in H_2O and (HNO_3 and HCl) up to 3 M, whereas the solid is moderately dissolved at 4 M HNO_3 and completely dissociated at 6 M, also the solid sample is stable in KOH up to 3 M, while partially dissociated at 4 M and fully dissociated at 6 M. The % solubility was raised by increasing of the acid and base concentrations [15]. Also, these results reflect that the sequence of stability of the studied composite is HCl ˃ HNO_3 ˃ KOH.

3.3 Sorption Results

3.3.1 Distribution Coefficients Studies (K_d)

Figure 5A, illustrates the variation of K_d for Pb(II), Cs(I), Cu(II), Cd(II), and Sr(II) ions onto P(AN-AM)-NS sorbent, as a function of pH. It is clear that the K_d rise by the increase in pH. The optimum K_d was achieved at pH 4.3 and was discovered to be (1655.6, 110.3, 91.7, 66.7, and 52.1 mL/g) for Pb(II), Cs(I), Cu(II), Cd(II), and Sr(II) ions, respectively. At a lower value ($pH \leq 3$), K_d was inhibited, related to the fact that when the pH is quite little, the existence of excess H^+ in solution which competes with Pb(II), Cs(I), Cu(II), Sr(II) and Cd(II) ions in the liquor and preferably occupy the binding positions available in P(AN-AM)-NS [42, 43]. At a higher value ($pH > 3$), K_d continuously rises with the increase in pH due to the reduction in H^+ competition and maximum uptake carried out at pH 4.3 as well as uptake was slightly decreased at $pH > 4.3$, so all sorption experiments were done at pH 4.3. K_d and α_b^a for the mentioned cations at different pHs (2.4–6) were calculated and tabulated in Table 2, and designated that the K_d have the affinity arrangement; Pb(II) > Cs(I) > Cu(II) > Cd(II) > Sr(II) ions, this arrangement supported that the sorption of studied cations was applied in hydrated ionic radii. The cations with minor hydrated ionic radii simply enter the cavities of the polymeric resin resulting in higher sorption [14]. Separation factors (α_b^a) were computed and designated that Pb(II) ion has very greater α_b^a by (31.8, 24.8, 18.1, and 15.0) for Sr(II), Cd(II), Cu(II), and Cs(I) ions at top uptake (pH 4.3), these values indicated that Pb(II) ions can simply separate from industrial and radioactive waste involved the above-mentioned cations.

The aqueous speciation distribution of Pb(II), Cs(I), Cu(II), Cd(II), and Sr(II) ions at ionic strength 0.001 was performed at tested pHs (2.4–6) and represented in Fig. 5B. The results showed that the speciation of Cs(I), Cd(II), and Sr(II) ions have no precipitate at tested pHs (2.4–6) with no presence of these ions in the hydroxide forms. While speciation distribution of Pb(II), and Cu(II) ions at tested

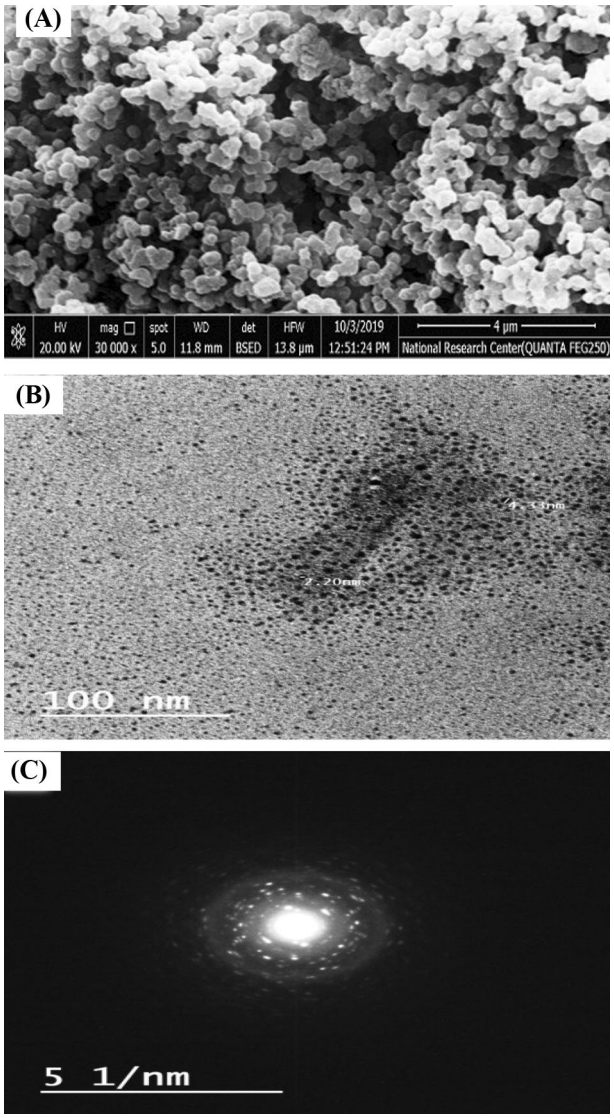

Fig. 4 **A** SEM micrograph, **B** and **C** TEM images of P(AN-AM)-NS nanocomposite

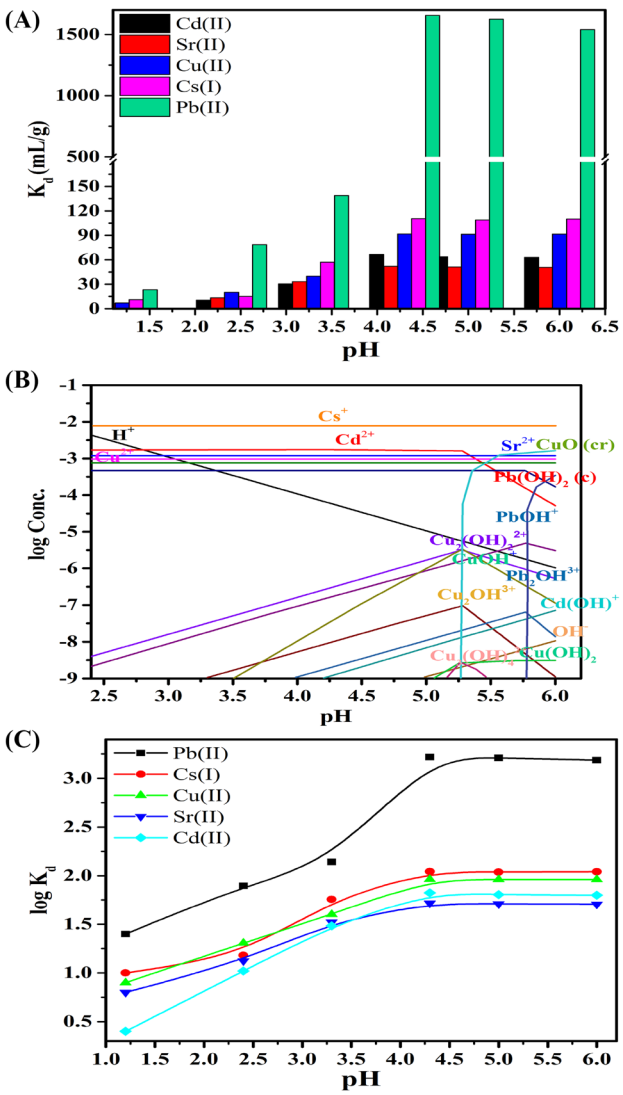

Fig. 5 **A** Effect of pH on K_d of various metal ions onto P(AN-AM)-NS at 25 ± 1 °C, **B** speciation of Pb^{2+}, Cs^+, Cu^{2+}, Sr^{2+} and Cd^{2+} ions at room temperature and 0.001 ionic strength, and **C** plots of log K_d against pH

Table 1 Chemical stability of P(AN-AM)-NS dissolved in different solvents for 4 days

The concentration of solvents (M)	% solubility			
	H_2O	HCl	HNO_3	KOH
0.5	Below detection limit	5.92	6	8
1		12.92	12.2	14.1
2		13.67	16.7	20.7
3		24.95	27.04	29.8
4		34.31	PD	PD
6		PD	CD	CD

PD partially dissolved, *CD* completely dissolved

pH (2.4–6) indicated that at pHs from 2.4 to 5 no precipitate occurred for these ions and the K_d values increase with increasing pH due to reducing competition between and H^+ ion in solution and Pb(II), and Cu(II) ions and maximum uptake was achieved at pH 4.3 while by increasing of pH above this value, Pb(II), and Cu(II) ions started to precipitate as $Cu_2(OH)_2^{2+}$, $Cu_2(OH)_2^{2+}$, Cu_2OH^{3+}, and $Cu_3(OH)_4^{2+}$ for Cu(II) ions and precipitate as $PbOH^+$, and Pb_2OH^{3+} for Pb(II), ions as present in Fig. 5B.

Figure 5C shows that the nonlinear relation between $logk_d$ and pH was observed for studied cations. This relation reflects the non-reality of the exchange mechanisms. This variation may be due to taking place reactions other than ion exchange, similar precipitation, and/or adsorption [15].

Table 2 K_d values and separation factors of various metal ions sorbed onto P(AN-AM)-NS at 25 ± 1 °C

pH	K_d (mL/g) and α	Sr(II)	Cd(II)	Cu(II)	Cs(I)	Pb(II)
1.2	K_d	6.3	2.7	7.1	11.1	23.3
	α_b^a		0.4	1.1	1.8	3.7
				2.6	4.1	8.6
					1.6	3.3
						2.1
2.4	K_d	13.3	10.4	20.3	15.2	78.6
	α_b^a		0.8	1.5	1.1	5.9
				2.0	1.5	7.6
					0.7	3.9
						5.2
3.3	K_d	33.3	30.4	40.0	57.1	138.7
	α_b^a		0.9	1.2	1.7	4.2
				1.3	1.9	4.6
					1.4	3.5
						2.4
4.3	K_d	52.1	66.7	91.7	110.3	1655.6
	α_b^a		1.3	1.8	2.1	31.8
				1.4	1.7	24.8
					1.2	18.1
						15.0
5	K_d	52.2	63.8	91.3	108.8	1625.0
	α_b^a		1.2	1.7	2.1	31.1
				1.4	1.7	25.5
					1.2	17.8
						14.9
6	K_d	50.9	62.9	91.5	109.9	1540.0
	α_b^a		1.2	1.5	1.7	24.5
				1.5	1.7	24.5
					1.2	16.8
						14.0

3.3.2 Influence of Shaking Time

The influence of shaking time changed from 15 min to 24 h on the removal efficiency of Pb^{2+}, Cs^+, Cu^{2+}, Sr^{2+}, and Cd^{2+} on P(AN-AM)-NS was done at fixed pH 4.3 and the experimental results are given in Fig. 6A, as a relation between removal efficiency percent and time. From this figure, it is clear that, as the mixing time increases from 15 to 4 h, the sorption percent of Pb^{2+}, Cs^+, Cu^{2+}, Sr^{2+}, and Cd^{2+} increased from about 68.2 to 98.6% for Pb^{2+}, from about 57.7 to 74.4% for Cs^+, from about 49.2 to 68.5% for Cu^{2+}, from about 56.6 to 64.3% for Sr^{2+}, and from about 34.5 to 48.8% for Cd^{2+}. Further, an increase in the mixing time up to 24 h does not affect the removal of Pb^{2+}, Cs^+, Cu^{2+}, Sr^{2+}, and Cd^{2+}. This means that the sorption equilibrium has been achieved at 4 h. Therefore, 4 h represents the preferred time to maximize the Pb^{2+}, Cs^+, Cu^{2+}, Sr^{2+}, and Cd^{2+} sorption using the synthesized P(AN-AM)-NS nanocomposite, and this time was used for further experimental work.

3.3.3 Kinetic Investigation

The Lagergren pseudo-first-order (PFO) equation is stated as [2, 44]:

$$\log (q_e - q_t) = -\left(\frac{K_f}{2.303}\right)t + \log q_e \quad (5)$$

In which K_f (min^{-1}) is a rate constant of PFO, q_e and q_t (mg/g) are the amount sorbed per gram at equilibrium and time t. Plotting log ($q_e - q_t$) beside t as exposed in Fig. 6B, the plot shows a linear relationship. The PFO suffered from lack when applied to Pb^{2+}, Cs^+, Cu^{2+}, Sr^{2+}, and Cd^{2+} sorption on the composite sorbent. When the q_e achieved from Lagergren plots was associated with the q_e (experimental) considered one of the main discrepancies was observed. Thus, good linearity of Lagergren plots is not promised that the reaction of Pb^{2+}, Cu^{2+}, Sr^{2+}, Cs^+, and Cd^{2+} with the sorbents don't follow PFO [45].

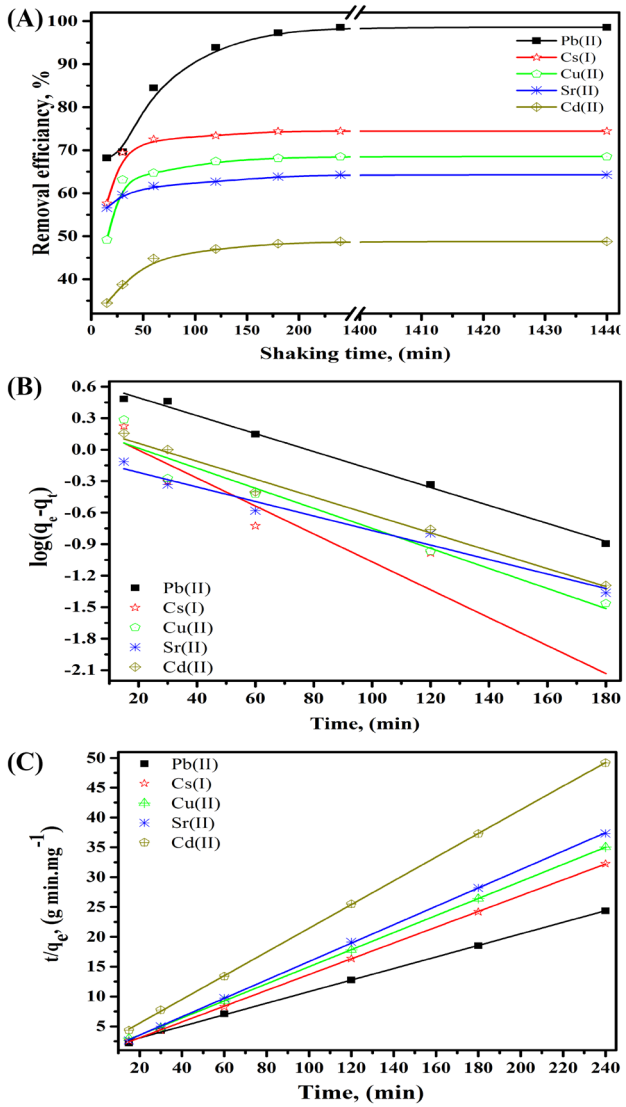

Fig. 6 Sorption of various metal ions on P(AN-AM)-NS at 25 ± 1 °C, **A** effect of shaking time on the removal efficiency, **B** pseudo-first-order kinetic plots, and **C** pseudo-second-order kinetic plots

The pseudo-second-order (PSO) could be exemplified by the subsequent equation [46]:

$$\frac{t}{q_e} = \frac{1}{K_s q_e^2} + \frac{t}{q_e} \quad (6)$$

where K_s is PSO rate constant (g mg^{-1} min^{-1}). Plots of t/q_t against t for Pb^{2+}, Cs^+, Cu^{2+}, Sr^{2+}, and Cd^{2+} removal are exposed in Fig. 6C. A linear relationship is achieved and R^2 nearer to unity and clarifies that the sorption procedure surveys PSO kinetics. The initial sorption rate represented as $h = K_s(q_e)^2$, q_e, K_s, and R^2 were computed and arranged in Table 3. These results reveal that R^2 is nearer to unity for PSO than PFO. The q_e is consistent with the q_e (experimental). So, the sorption interaction can be approached more agreeably by the PSO. These data reveal that PSO is the chief interaction and K_s of Pb^{2+}, Cs^+, Cu^{2+}, Sr^{2+}, and Cd^{2+} performs to be exact by the chemisorption method [46].

3.3.4 Sorption Mechanism

Scheme 1 illustrates the sorption mechanism of Pb^{2+}, Cs^+, Cu^{2+}, Sr^{2+}, and Cd^{2+} onto P(AN-AM)-NS at desired pH (4.3). All investigated cations are present at this pH value in metal cation forms not found as metal hydroxide forms according to the data obtained from the speciation of these ions. From the results exposed in Scheme 1, the sorption mechanism of monovalent Cs^+ ion onto P(AN-AM)-NS was achieved by an exchange reaction between Cs^+ with one hydrogen atom of hydroxyl group binding with the silicon atom. Whereas in the case of bivalent metal ions (Pb^{2+}, Cu^{2+}, Sr^{2+}, and Cd^{2+} ions) onto P(AN-AM)-NS the sorption mechanism was achieved by an exchange reaction between bivalent metal ions with two hydrogen atoms of hydroxyl group binding with the silicon atom [47] as exposed in Scheme 1.

3.3.5 Capacity Measurements and Thermal Stability

Heating temperatures affected the capacity of Pb^{2+}, Cs^+, Cu^{2+}, Sr^{2+}, and Cd^{2+} onto P(AN-AM)-NS in H^+ form was achieved, and the results were formulated in Table 4. The prominent reduction in the capacity was noticed with heating

Table 3 Kinetic parameters of various metal ions on P(AN-AM)-NS at 25 ± 1 °C

Metal ions sorbed	Pseudo-first-order kinetics			Pseudo-second-order kinetics				q_e, exp. (mg/g)
	$k_f \times 10^{-3}$	q_e (mg/g)	R^2	$K_s \times 10^{-3}$	$h \times 10^{-2}$	q_e (mg/g)	R^2	
Pb(II)	− 8.6	4.63	0.993	8.2	88.4	10.32	0.999	9.86
Cs(I)	− 13.3	1.83	0.911	39.4	225.3	7.56	0.999	7.4
Cu(II)	− 9.5	1.60	0.931	29.9	146.6	6.99	0.999	6.9
Sr(II)	− 6.9	0.83	0.959	53.6	225.8	6.48	0.999	6.4
Cd(II)	− 8.5	1.7	0.981	25.3	64.1	5.03	0.999	4.9

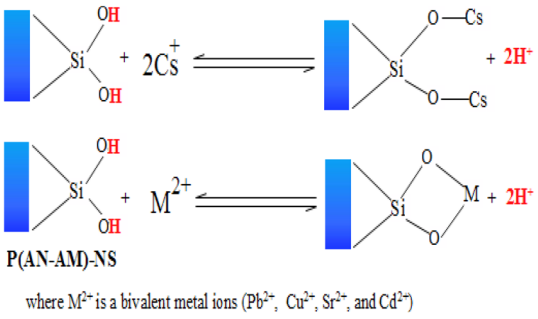

Scheme 1 Sorption mechanism of Pb^{2+}, Cs^{+}, Cu^{2+}, Sr^{2+}, and Cd^{2+} ions onto P(AN-AM)-NS

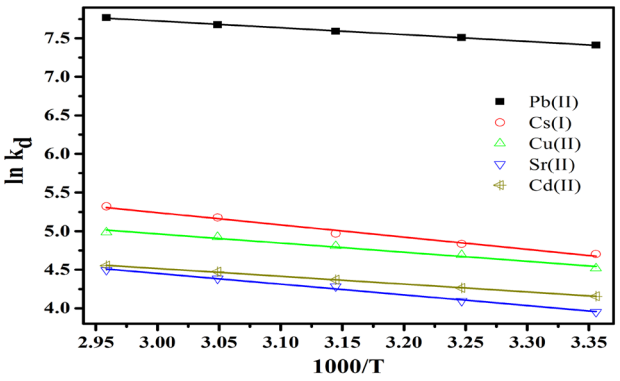

Fig. 7 Van't Hoff plot of the adsorption of various metal ions on P(AN-AM)-NS

temperatures, corresponding to decay of the organic fragment of the solid as exposed in TGA and DTA data [5]. The capacity increases according to reduction in the hydrated ionic radii and hydration energy with sequence order; $Pb^{2+} > Cs^{+} \gg Cu^{2+} > Sr^{2+} > Cd^{2+}$ [48, 49]. The little capacity of this material for Cd^{2+} reflects the non-selectivity for this ion [15]. The data present in Table 4 reflect the very high sorption capacity for studied cations sorbed onto P(AN-AM)-NS indicated that an improvement in ion sorption performance of P(AN-AM)-NS initiated by gamma-irradiation. Comparison of the monolayer capacity of Pb^{2+}, Cs^{+}, Cu^{2+}, Cd^{2+}, and Sr^{2+} onto P(AN-AM)-NS with other sorbents obtained in the literature is listed in Table 5. It can be seen that the prepared P(AN-AM)-NS composite has a higher sorption capacity than many other sorbents. It shows that P(AN-AM)-NS can be considered as a promising material for removal of Pb^{2+}, Cs^{+}, Cu^{2+}, $Cd^{2+}$and Sr^{2+} ions from waste solution.

3.3.6 Thermodynamic Studies

Figure 7 displays the linear relation among $\ln k_d$ of Pb^{2+}, Cs^{+}, Cu^{2+}, Sr^{2+}, and Cd^{2+} on P(AN-AM)-NS and 1000/T agreeing to the Van't Hoff equation [44];

$$\ln K_d = \frac{\Delta S^{\circ}}{R} - \frac{\Delta H^{\circ}}{RT} \tag{7}$$

Table 4 Effect of heating temperatures on the capacity of P(AN-AM)-NS for various metal ions

Heating temperature, °C	Weight loss (%)	Pb(II)		Cs(I)		Cu(II)		Sr(II)		Cd(II)	
		IEC	% R	IEC	% R	IEC	% R	IEC	% R	IEC	% R
50	Nil	101.7	100	94.3	100	57.6	100	54.3	100	33.4	100
100	6.18	94.0	92.4	89.1	94.5	50.0	86.8	42.5	78.3	26.0	77.8
200	7.6	83.1	81.7	74.7	79.2	37.2	64.6	35.0	64.5	21.8	65.3
400	49.8	72.8	71.6	61.5	65.2	25.5	44.3	25.0	46.0	12.4	37.1

where IEC is ion exchange capacity (mg/g) and % R is Retention of ion exchange capacity

Table 5 Comparison of sorption capacities of Pb(II), Cs(I), Cu(II), Cd(II), and Sr(II) on different sorbents under different conditions

Sorbents	pH	Capacity (mg/g)					References
		Pb(II)	Cs(I)	Cu(II)	Cd(II)	Sr(II)	
P(AN-AM)-NS	4.3	101.7	94.3	57.6	54.3	33.4	Present work
Polyacrylamide Sn(IV) molybdophosphate	4.5	176.1	158.2	30.8	78.7	–	[50]
Polyacrylamide thorium(IV) phosphate	7.0	644.2	–	–	–	317.4	[51]
Polyacrylamide titanium tungstophosphate	4.61	–	366.8	–	–	–	[52]
Polypyrrole thorium(IV) phosphate	6.3	–	–	–	–	82.80	[53]
Acrylamide zirconium(IV) sulphosalicylate	6.5	–	–	–	–	135.8	[54]
Phosphate-modified montmorillonite	> 11	–	59.27	–	–	11.04	[55]
Polyacrylamide Sn(IV) silicate	4.0	–	0.32	–	1.23	2.2	[56]
Polyacrylamide Sn(IV) antimonite	4.0	–	0.47	–	1.73	3.7	[56]

Table 6 Thermodynamic parameters for adsorption of various metal ions on P(AN-AM)-NS

Metals sorbed	Temp (K)	ΔH° (kJ/mol)	ΔS° (J/mol K)	ΔG° (kJ/mol)
Pb(II)	298	7.4	86.4	− 18.4
	308			− 19.2
	318			− 20.1
	328			− 21.0
	338			− 21.8
Cs(I)	298	13.2	83.2	− 11.6
	308			− 12.4
	318			− 13.3
	328			− 14.1
	338			− 14.9
Cu(II)	298	9.9	70.9	− 11.3
	308			− 12.0
	318			− 12.7
	328			− 13.4
	338			− 14.1
Sr(II)	298	11.5	71.6	− 9.8
	308			− 10.5
	318			− 11.2
	328			− 12.0
	338			− 12.7
Cd(II)	298	8.4	62.8	− 10.3
	308			− 10.9
	318			− 11.6
	328			− 12.2
	338			− 12.8

where ΔS°, ΔH°, R, and T are the change of entropy, the change of enthalpy, the gas constant, and absolute temperature, respectively. K_d of investigated cations improved with rising temperatures (298–338 K) (i.e., the K_d reduced with raising 1000/T) as exposed in Fig. 7. This enhancement in sorption was corresponding to the quickening of some firstly slow adsorption phases and the creation of some fresh exchangeable sites on the sorbent layers [44]. From the slopes and intercepts displayed in Fig. 7, ΔH° and ΔS° were assessed and arranged in Table 6. The positive values of both ΔH° and ΔS° indicate the endothermic nature of the sorption process and the bigger randomness of solid solution interface in the adsorption of these cations on P(AN-AM)-NS, respectively [44].

The change of free energy ΔG° was computed by the equation:

$$\Delta G^{\circ} = \Delta H^{\circ} - T\Delta S^{\circ} \quad (8)$$

$$\Delta S^{\circ} = TR \ln K_d \quad (9)$$

The negative values of ΔG° represented in Table 6 reflect that the sorption is spontaneous and reveal the better sorption of these ions on P(AN-AM)-NS compared with H^+ ion [44].

4 Conclusion

Polyacrylonitrile acrylamide nano-silica was fabricated, characterized, and employed for batch sorption of lead, cesium, copper, strontium, and cadmium ions from a liquid medium. P(AN-AM)-NS fabricated by γ-radiation initiated preparation at 50 kGy. The optimal sorption parameters for ion sorption were given at pH 4.3, and equilibrium time at 4 h. The distribution coefficients at optimum pH have selectivity order: $Pb^{2+} > Cs^{+} > Cu^{2+} > Cd^{2+} > Sr^{2+}$. The systems kinetic follow pseudo-second-order kinetics. The capacity of studied cations reveals that P(AN-AM)-NS has affinity sequence; $Pb^{2+} > Cs^{+} \gg Cu^{2+} > Sr^{2+} > Cd^{2+}$. Finally, thermodynamic parameters showed that the sorption interaction was spontaneous and endothermic.

Acknowledgements This work has been supported by the Egyptian Atomic Energy Authority. Great thanks to all members of the nuclear fuel technology department, Egyptian Atomic Energy Authority for supporting this work.

Author Contributions MRA: data curation, writing—original draft review and editing. EHEM: experimental work and editing. WMEK: experimental work and reviewing.

Declarations

Conflict of interest The author declare that they have no conflict of Interest.

References

1. V.K. Gupta, S. Agarwal, D. Pathania, N.C. Kothiyal, G. Sharma, Carbohydr. Polym. **96**, 277 (2013)
2. M.R. Abass, E.H. EL-Masry, A.B. Ibrahim, Environ. Geochem. Health **43**, 3169 (2021)
3. M.R. Abass, A.B. Ibrahim, M.M. Abou-Mesalam, Chem. Pap. **75**, 3751 (2021)
4. D. Pathania, G. Sharma, A. Kumar, N.C. Kothiyal, J. Alloys Compd. **588**, 668 (2014)
5. V.K. Gupta, S. Agarwal, I. Tyagi, D. Pathania, B.S. Rathore, G. Sharma, Ionics (Kiel). **21**, 2069 (2015)
6. V.K. Gupta, G. Sharma, D. Pathania, N.C. Kothiyal, J. Ind. Eng. Chem. **21**, 957 (2015)
7. D. Pathania, G. Sharma, M. Naushad, V. Priya, Desalin. Water Treat. **57**, 468 (2016)
8. A.A. Khan, L. Paquiza, Desalination **265**, 242 (2011)
9. M.M. Abou-Mesalam, M.R. Abass, A.B. Ibrahim, A.M. Elseman, A.M. Hassan, Bull. Mater. Sci. **42**, 31 (2019)
10. B.J. Sanghavi, S.M. Mobin, P. Mathur, G.K. Lahiri, A.K. Srivastava, Biosens. Bioelectron. **39**, 124 (2013)

11. R.F. Aglan, M.M. Hamed, Russ. J. Appl. Chem. **87**, 373 (2014)
12. M.M. Hamed, J. Radioanal. Nucl. Chem. **302**, 303 (2014)
13. M.M. Hamed, S.M. Yakout, H.S. Hassan, J. Radioanal. Nucl. Chem. **295**, 697 (2013)
14. M.M. Abou-Mesalam, M.R. Abass, A.B. Ibrahim, E.S. Zakaria, Desalin. Water Treat. **193**, 402 (2020)
15. M.M. Abou-Mesalam, M.R. Abass, M.A. Abdel-Wahab, E.S. Zakaria, A.M. Hassan, Desalin. Water Treat. **109**, 176 (2018)
16. E. Skwarek, Adsorpt. Sci. Technol. **33**, 575 (2015)
17. M.H. Taha, A.M. Masoud, Y.M. Khawassek, A.E.M. Hussein, H.F. Aly, E. Guibal, Environ. Sci. Pollut. Res. **27**, 31278 (2020)
18. E. Skwarek, W. Janusz, Sep. Sci. Technol. **51**, 11 (2016)
19. O. Rosskopfová, M. Galamboš, P. Rajec, J. Radioanal. Nucl. Chem. **287**, 715 (2011)
20. P.A. Kavaklı, C. Kavaklı, N. Seko, M. Tamada, O. Güven, Radiat. Phys. Chem. **127**, 13 (2016)
21. H. El-Didamony, E. El-Fadaly, A.A. Amer, I.H. Abazeed, Boletín La Soc, Española Cerámica y Vidr. **59**, 31 (2020)
22. M.M. Hamed, A.M. Shahr El-Din, E.A. Abdel-Galil, J. Radioanal. Nucl. Chem. **322**, 663 (2019)
23. A.B. Ibrahim, M.R. Abass, E.H. EL-Masry, M.M. Abou-Mesalam, Appl. Radiat. Isot. **178**, 109956 (2021)
24. M.M. Hamed, S.E. Rizk, A.A. Nayl, Part. Sci. Technol. **34**, 716 (2016)
25. M.M. Abass, A.B. Ibrahim, E.H. EL-Masry, M.M. Abou-Mesalam, J. Radioanal. Nucl. Chem. **329**, 849 (2021)
26. M.R. Abass, H.M. Diab, M.M. Abou-Mesalam, Silicon **1**, 6 (2021)
27. S. Lee, J. Kim, B.-C. Ku, J. Kim, H.-I. Joh, Adv. Chem. Eng. Sci. **02**, 275 (2012)
28. M. Afifi, M.R. Abass, H.M. Diab, M.M. Abou-Mesalam, M.S. Gaafar, Silicon (2021). https://doi.org/10.1007/s12633-021-01229-7
29. W. Zhu, Z. Yang, A. Yasin, Y. Liu, L. Zhang, Materials (Basel) **14**, 3277 (2021)
30. Q. Zhao, T. Cao, Ind. Eng. Chem. Res. **51**, 4952 (2012)
31. A.S. Dawood, Y. Li, Polish. J. Environ. Stud. **23**, 43 (2014)
32. M.M. Abou-Mesalam, M.R. Abass, M.A. Abdel-Wahab, E.S. Zakaria, A.M. Hassan, H.F. Khalil, Desalin. Water Treat. **57**, 25757 (2016)
33. M.F. Hassan, S.Z.M. Yusof, Microsc. Res. **2**, 30 (2014)
34. E.H. Borai, M.G. Hamed, A.M. El-Kamash, T. Siyam, G.O. El-Sayed, New J. Chem. **39**, 7409 (2015)
35. A. Nilchi, A. Khanchi, H. Atashi, A. Bagheri, L. Nematollahi, J. Hazard. Mater. **137**, 1271 (2006)
36. Y.F. El-Aryan, E.A. Abdel-Galil, G.E.S. El-deen, Russ. J. Appl. Chem. **88**, 516 (2015)
37. K.M. Abualnaja, A.E. Alprol, M.A. Abu-Saied, A.T. Mansour, M. Ashour, Nanomaterials **11**, 1144 (2021)
38. P. Bhardwaj, S. Singh, V. Singh, S. Aggarwal, U.K. Mandal, Int. J. Polym. Mater. **57**, 404 (2008)
39. S.N.A.M. Jamil, M. Khairuddin, R. Daik, E-Polymers **15**, 45 (2015)
40. W.P.S.L. Wijesinghe, M. Mantilaka, T. Karunarathne, R.M.G. Rajapakse, Nanoscale Adv. **1**, 86 (2019)
41. B.A. Carter, D.B. Williams, C.B. Carter, D.B. Williams, *Transmission Electron Microscopy: A Textbook for Materials Science. Diffraction. II* (Springer, New York, 1996)
42. S.S. Metwally, H.S. Hassan, N.M. Samy, J. Mol. Liq. **287**, 110941 (2019)
43. E.A. Abdel-Galil, A.B. Ibrahim, W.M. El-Kenany, Desalin. Water Treat. (2021). https://doi.org/10.21203/rs.3.rs-809665/v1
44. E.A. Abdel-Galil, A.B. Ibrahim, M.M. Abou-Mesalam, Int. J. Ind. Chem. **7**, 231 (2016)
45. R.R. Sheha, A.A. El-Zahhar, J. Hazard. Mater. **150**, 795 (2008)
46. E.H. Borai, M.F. Attallah, A.H. Elgazzar, A.S. El-Tabl, Part. Sci. Technol. **37**, 414 (2019)
47. G. Zhao, X. Huang, Z. Tang, Q. Huang, F. Niu, X. Wang, Polym. Chem. **9**, 3562 (2018)
48. N. Rahman, U. Haseen, M. Rashid, Arab. J. Chem. **10**, S1765 (2017)
49. A.P. Gupta, H. Agarwal, S. Ikram, J. Indian Chem. Soc. **80**, 57 (2003)
50. I.M. El-Naggar, E.A. Mowafy, E.A. Abdel-Galil, M.F. El-Shahat, Glob. J. Phys. Chem. **1**, 91 (2010)
51. M. Islam, R. Patel, J. Hazard. Mater. **156**, 509 (2008)
52. E.A. Abdel-Galil, G.E.S. El-Deen, Y.F. El-Aryan, M. Khalil, Russ. J. Appl. Chem. **89**, 467 (2016)
53. A.A. Khan, Inamuddin, M.M. Alam, React. Funct. Polym. **63**, 119 (2005)
54. S. Ahad, A. Bashir, T. Manzoor, A.H. Pandith, RSC Adv. **6**, 35914 (2016)
55. B. Ma, S. Oh, W.S. Shin, S.-J. Choi, Desalination **276**, 336 (2011)
56. I.M. El-Naggar, G.M. Ibrahim, E.A. El-Kady, Adv. Chem. Eng. Sci. **2**, 180 (2012)

Authors and Affiliations

Mohamed Ragab Abass[1] · Eman Hassan EL-Masry[1] · Wafaa Mohamed El-Kenany[1]

Mohamed Ragab Abass
mohamed.ragab2014300@yahoo.com;
mohamed.r.abass@eaea.org.eg

Wafaa Mohamed El-Kenany
wafaamohamed4312@yahoo.com;
w_mohamed13@yahoo.com

[1] Hot Laboratories, and Waste Management Center, Egyptian Atomic Energy Authority, Cairo 13759, Egypt